J. Physiol. (1987), **393**, *pp.* 437–466
With 12 text-figures
Printed in Great Britain

ACTIVATION OF THE PRIMARY KINETIC MODES OF LARGE- AND SMALL-CONDUCTANCE CHOLINERGIC ION CHANNELS IN *XENOPUS* MYOCYTES

BY ANTHONY AUERBACH* AND CHRISTOPHER J. LINGLE†

*From the * Department of Biophysical Sciences, State University of New York at Buffalo, Buffalo, NY and the † Department of Biological Sciences and Institute of Molecular Biophysics, Florida State University, Tallahassee, FL, U.S.A.*

(*Received 13 January 1987*)

SUMMARY

1. The kinetic properties of single acetylcholine (ACh)-activated ion channels in tissue-cultured *Xenopus* myocytes have been examined in cell-attached patches. The rates of agonist binding and channel gating were inferred from the durations of open and closed intervals from channels exposed to 40 nM–200 μM-ACh. The predominant kinetic forms of large- (γ_{60}) and small-conductance (γ_{40}) cholinergic channels were compared.

2. At high [ACh], bursts were defined so that they primarily reflect sojourns in activatable states. The probability that a channel is open within a burst (P_o) increases between 2 and 200 μM-ACh. P_o is half-maximal at ~ 5 μM for γ_{40} channels and at ~ 25 μM for γ_{60} channels.

3. Open interval durations for γ_{40} channels are distributed as the sum of two exponentials, with the slow component ($\tau \sim 2{\cdot}8$ ms) accounting for $> 80\%$ of the total. Open interval durations for γ_{60} channels are often distributed as a single exponential with an apparent time constant of $\sim 0{\cdot}8$ ms. For both conductance forms of channel, open interval durations show no significant dependence on [ACh] in the range 0·04–10 μM, but decrease at higher [ACh] in a manner consistent with channel block by agonist molecules.

4. Closed interval durations within bursts (2–100 μM-ACh) for γ_{60} or γ_{40} channels are described by the sum of two or three exponentials. For both conductance forms of channel the apparent time constant of the fastest component is ~ 40 μs and does not change significantly with [ACh], and the time constant of the predominant, slowest component (τ_{slow}) decreases with increasing [ACh].

5. For γ_{40} channels, at high [ACh] τ_{slow} saturates at $\sim 0{\cdot}17$ ms, while no saturation is apparent for γ_{60} channel τ_{slow} values up to 200 μM-ACh. Below 50 μM-ACh, γ_{40} τ_{slow} values are $\sim 1{\cdot}5$ times shorter than γ_{60} values.

6. Estimates of rate constants for agonist binding and channel gating were obtained by fitting closed interval durations in the range 2–100 μM-ACh. γ_{60} channels have a > 5-fold faster opening rate, ~ 10-fold faster closing rate, and ~ 3-fold lower affinity than do γ_{40} channels. There is some indication of positive co-operativity of ACh binding to γ_{40} channels.

INTRODUCTION

Nicotinic acetylcholine receptors are a family of ion channel proteins that share at least two basic features: receptor sites that bind a common set of agonists and antagonists, and an ion-conducting pathway that discriminates poorly between monovalent cations. In some preparations, such as the mouse cell line BC_3H1 (Sine & Steinbach, 1986) and the adult vertebrate neuromuscular junction (Colquhoun & Sakmann, 1985), nicotinic cholinergic channels appear to be functionally homogeneous. In particular, acetylcholine receptor channels at the adult vertebrate end-plate are viewed as the end-point of a vectorial pathway of molecular differentiation. In other less differentiated or less specialized preparations, based on the properties of apparent open channel lifetime and conductance, more than one kind of cholinergic nicotinic channel may be expressed. For example, at least two basic classes of cholinergic channels have been described not only in many vertebrate embryonic and denervated skeletal muscle cells, but also in end-plates from old rats (Smith, 1986) and in certain adult twitch and slow muscle fibre end-plates (Dionne, 1986). Changes in the proportions of functionally distinct cholinergic channels during synapse assembly, maturation, and ageing have been observed in muscle cells (reviewed by Schuetze & Role, 1987) and as a consequence of the nature of the innervating presynaptic cell in sympathetic neurones (Marshall, 1985).

The functional heterogeneity of nicotinic cholinergic receptors in developing and denervated muscle has been well documented with regard to both the rates of conductance and apparent mean open channel lifetime. Vertebrate embryonic or denervated muscle cells have two classes of nicotinic channel which differ in conductance by a factor of $\sim 1{\cdot}5$ (Katz & Miledi, 1972). In all vertebrate muscle cells where it has been examined (except chick; Scheutze, 1980), the larger-conductance channel has an apparent open channel lifetime which is ~ 3 times shorter than the small-conductance form of channel. Recently, it has been observed that within each conductance class cholinergic channels can also be functionally diverse. In *Xenopus* myocytes, both large- and small-conductance channels are expressed in a variety of kinetically distinct forms (Leonard, Nakajima, Nakajima, & Takahashi, 1984; Auerbach & Lingle, 1986*b*). Multiple kinetic classes of cholinergic channels with similar conductance have also been reported in rat myotubes (Jackson, 1984).

These variations in channel function are presumably manifestations of differences in protein and/or membrane structure. One key question is whether kinetically distinct forms of channel reflect differences in polypeptide sequence, subunit composition or post-translational modifications of the receptor–channel complex. Subunit substitution studies in the *Xenopus* oocyte expression system have suggested that the major differences in channel conductance and apparent lifetime between the two predominant classes of neuromuscular channel can be attributed to replacement of a single subunit (Mishina, Takai, Imoto, Noda, Takahashi, Numa, Methfessel & Sakmann, 1986). However, this explanation can certainly not account for all of the heterogeneity within a single conductance class of channel as observed in *Xenopus* myocytes. In addition, the existence of such heterogeneity indicates that comparison of channel function based solely on apparent mean open time and conductance may not reveal the full extent of functional differences.

Although much can be learned from studying the properties of experimentally assembled channels, a complete understanding of nicotinic acetylcholine receptor channel function will continue to require a complete characterization of each of the many functional forms of the channel that may be expressed in normal cells. These functional properties are best expressed not simply in terms of channel lifetime and conductance, but also in terms of the rates of agonist association/dissociation, channel opening/closing, and desensitization/resensitization.

Towards this end we have compared the kinetic properties of the most common kinetic forms of large- and small-conductance cholinergic channels in aneural cultures of *Xenopus* myocytes in terms of the rate constants which underlie agonist binding and channel gating. The results indicate that these forms of cholinergic channel differ both in their affinity for ACh and in their rates of channel opening and closing. Some results have appeared in abstract form (Auerbach & Lingle, 1986*a*, 1987).

METHODS

The details of culture preparation, electrophysiology, and data analysis have been described previously (Auerbach & Lingle, 1986*b*).

Preparation of cultures. Somites from stage 18–21 embryos were separated from surrounding yolk, notocord and spinal cord by incubation in a low Ca^{2+}–collagenase (1 mg/ml; Sigma type 1A) solution. Myocytes were dissociated from somites by incubation in a divalent cation-free–trypsin (0·05 mg/ml; Gibco) solution. In general, the cultures were maintained for a total time of 12–48 h at room temperature in 60% (v/v) L-15, 8 mM-HEPES, 0·5% (v/v) horse serum, and 1 μg gentamycin/ml. For the electrophysiological experiments, the culture medium was replaced over a period of about 30 min with saline containing 100 mM-NaCl, 1·6 mM-KCl, 1·0 mM-$CaCl_2$ and 10 mM-Na HEPES, pH 7·4.

Electrophysiology. Standard methods for cell-attached recording of single-channel currents were employed (Hamill, Marty, Neher, Sakmann & Sigworth, 1981). The patch pipette contained physiological saline plus AChCl. The temperature was 23–26 °C.

The potential of the patch pipette was held at +40 mV. The membrane potential was inferred from the amplitudes of single-channel currents. For small-conductance channels, in fifty-eight patches which were analysed for kinetic parameters the mean single-channel current amplitude was $5{\cdot}10 \pm 0{\cdot}52$ pA (mean ± S.D.). For large-conductance channels, forty-five patches were analysed and the mean current amplitude was $7{\cdot}12 \pm 1{\cdot}05$ pA. Assuming a linear current–voltage relationship, conductances of 45 and 64 pS for large- and small-conductance channels, and a zero-current potential of −5 mV (Brehm, Kullberg & Moody-Corbett, 1984), these amplitudes indicate that in our experiments the membrane potential averaged −117 mV and was in the range −100 to −130 mV.

Single-channel currents were recorded on an analog magnetic tape-recorder (Racal) with a bandwidth of d.c.-5 kHz (3 db; 4-pole Bessel). Except where indicated, the data were digitized at 40 kHz (IBM PC/AT or Data General Eclipse) and were analysed without further low-pass filtering. In some cases the data were sampled at 10 kHz and the bandwidth was further limited by invoking a finite impulse response (FIR) digital Gaussian filter (Colquhoun & Sigworth, 1983) having a 3-db cutoff of 3 kHz, yielding an effective system bandwidth (f_c) of 2·6 kHz.

Burst selection. In *Xenopus* myocytes, cholinergic channels of similar conductance can be heterogeneous with regard to activation kinetic properties (Auerbach & Lingle, 1986*b*), and an essential aspect of the analysis was to isolate bursts arising from an apparently homogeneous population of ACh-activated channels.

First, an automated pattern-recognition program (IPROC; Sachs, Neil & Barkakati, 1982) identified channel opening and closing transitions and generated an 'events list' containing the starting locations and mean amplitudes of open and closed intervals. The determination of the mean amplitude of an event included a settling time allowance of $0{\cdot}6/f_c$, usually equal to six samples (150 μs). Events shorter than twice the settling allowance were considered to be of indeterminate

amplitude and were noted as such in the events list. Next, a single-channel database manager (LPROC; J. Neil, unpublished) operated on the events list to generate a 'burst list'. Bursts were defined as groups of open intervals separated by closed intervals less than some critical value, τ_{crit}. At high concentrations of ACh (2–200 μM), τ_{crit} was determined by fitting the unconditional closed interval distribution for the entire record to the sum of three to six exponentials; one component usually accounted for > 60% of all closed intervals in a record, and τ_{crit} was set to be at least 3 times this value. τ_{crit} values ranged from 10–500 ms, but were usually 10 or 20 ms. At low ACh concentrations (40–200 nM), τ_{crit} was 2 or 3 ms. For each burst in the list a number of parameters were noted, including the starting location, duration, mean amplitude, probability of being open within the burst (P_o), mean open interval duration, mean closed interval duration and number of open intervals in the burst. Bursts with less than five open intervals, and bursts containing an interval where more than one channel was open simultaneously, were excluded from the list.

The parameters in the burst list served as guides to select specific kinetic and conductance populations of events for further analysis. For each patch event amplitude and burst P_o histograms were compiled and the distributions were fitted by Gaussian functions. Bursts with amplitudes *and* P_o values within two or three S.D. of the distribution means were considered to represent a single population, and open or closed intervals from these bursts were selected for further analysis. Histograms of the durations of open or closed intervals were compiled and were fitted to the sum of one to four exponentials. Because interval durations measured at half-amplitude are biased for short-lived events (Sachs & Auerbach, 1983; Sine & Steinbach, 1986), intervals shorter than $0{\cdot}5/f_c$ (usually 100 μs) were excluded from the fit.

Curve fitting. All distributions were fitted with a non-linear, least-squares algorithm (subroutine RMSSQ or ZXSSO, from International Mathematics and Statistics Library, Houston, TX, U.S.A.), as described previously (Sachs & Auerbach, 1983). When interval duration or current amplitude histograms were fitted, the residuals were weighted for counting statistics, i.e. inversely with the number of counts in each bin. When fitting characteristic time–rate constants as a function of [ACh] (Figs 6 and 9), the residuals were weighted inversely by the standard error of the mean for each value.

Missed events correction. The apparent durations of open (and closed) intervals are overestimates of the true durations because some short-lived closed (and open) events do not reach half-amplitude and are not detected. We determined the minimum duration event to reach half-amplitude (τ_d) by passing pulses through the tape-recorder–filter combination. The measured value of τ_d was $\sim$ 35 μs, close to the value calculated for a bandwidth of 5 kHz (Colquhoun & Sigworth, 1983). It is possible, however, that τ_d varied on a patch-to-patch basis depending on the seal characteristics.

We made a first-order correction for missed events from distributions which are distributed as the sum of k exponential components by weighting the probability of capturing an event from each component (F_i) by the probability of getting an event from that component (P_i):

$$F_i = \exp(-\tau_d/\tau_i)$$

$$F^* = \sum_{i=1}^{k} F_i P_i$$

where τ_i is the time constant of the ith component. P_i was determined from the fit of the intraburst interval duration histograms and was equal to the fraction of all events belonging to the ith component. F^*, the estimated fraction of events which reached half-amplitude and were therefore captured, was calculated separately for both open and closed intervals. For example, in the file shown in Figs 2 and 3 (10 μM-ACh; kinetic parameters given in Table 1) we estimate that for γ_{40} channels 88% of open and 74% of closed intervals were captured, and for γ_{60} channels 84% of open and 74% of closed intervals were captured.

The estimated fraction of events which were captured was used to correct the observed durations of the predominant, slowest component of open and closed intervals:

$$\tau^{corr}_{closed} = \tau^{obs}_{closed} F^*_{open}$$

$$\tau^{corr}_{open} = \tau^{obs}_{open} F^*_{closed}$$

where τ^{corr} and τ^{obs} refer to the corrected and observed values of the time constant of the slowest component in the open–closed interval duration distributions. The correction procedure was applied on a file-by-file basis.

Fast openings accounted for < 20% of the total and were usually more than 5 times longer than τ_d, so few of these events were missed and the closed interval durations were relatively unchanged by the above correction procedure. Fast closures, however, were about equal in duration to τ_d and were more often missed. Consequently, corrected open interval durations were less than the observed values, particularly at high ACh concentrations where fast closures were common. Typical magnitudes of the correction can be seen in Tables 1 and 2.

TABLE 1. Kinetic parameters of bursts at 10 μM-ACh

		Single patch		Combined patches				
		Uncorrected		Uncorrected			Corrected	
	Parameter	Value	c.l.	Mean	S.D.	N	Mean	S.D.
γ_{40} open	τ_{fast}	0·54	0·07	0·35	0·12	5		
	τ_{slow}	2·65	0·12	3·09	1·06	6	2·46	1·04
	f_{slow}	0·83	0·07	0·92	0·05	6		
γ_{40} closed	τ_{fast}	0·030	0·002	0·037	0·010	6		
	τ_{med}	0·31	0·10	0·43	0·36	3		
	τ_{slow}	1·89	0·05	1·99	0·29	6	1·95	0·29
	f_{slow}	0·60	0·05	0·58	0·12	6		
	f_{med}	0·05	0·02	0·08	0·09	6		
γ_{60} open	τ_{fast}	0·29	0·06	0·22	0·10	3		
	τ_{slow}	0·80	0·08	0·68	0·01	5	0·60	0·08
	f_{slow}	0·83	0·10	0·87	0·14	5		
γ_{60} closed	τ_{fast}	0·025	0·003	0·028	0·010	5		
	τ_{med}	0·25	0·11	0·49	0·11	3		
	τ_{slow}	3·26	0·05	4·19	1·44	5	3·91	1·29
	f_{slow}	0·65	0·03	0·62	0·23	5		
	f_{med}	0·02	0·02	0·02	0·02	5		

The time constants are given in milliseconds; c.l. are the 90% confidence limits on the parameter; uncorrected/corrected refers to whether or not the missed events correction was invoked (see Methods). The open and closed interval parameters are for the intraburst events only. f is the fraction of all open or closed intervals belonging to the specified component. N, number of patches.

TABLE 2. Kinetic parameters of bursts at 40–200 nM-ACh

	γ_{40}			γ_{60}*	
	Mean	S.D.	N	Value	c.l.
$\tau_{closed,fast}$	0·041	0·016	16	0·024	0·057
τ_{open}(U)	3·37	0·64	16	0·93	0·36
τ_{open}(C)	2·90	0·59	16	0·72	—
τ_{burst}	4·09	0·96	16	1·10	0·05
Open intervals/burst (U)	1·20	0·13	16	1·18	—
Open intervals/burst (C)	1·40	0·22	16	1·53	—
Fast closed intervals/burst	0·57	0·53	16	0·58	—

Time constants are in milliseconds; all references to open intervals and bursts are to the slow component only. * The intervals were pooled from thirteen different patches. C and U refer to estimates which have or have not been corrected for missed events. N, number of patches; c.l., 90% confidence limits.

The above correction is only an approximate solution to the missed events problem because it assumes: (1) that the durations of missed events are negligible compared to the interval in which they occur, (2) that only slow interval durations are substantially biased by missed events, (3) that events occur within slow intervals at the same relative frequency they do within bursts, and, most importantly, that (4) the time constants and relative proportions of events determined from the fit

to intraburst interval duration distributions are accurate. Exact solutions to the missed events problem for specific kinetic models have been described by Colquhoun & Sigworth, (1983) Roux & Sauve (1985) and Blatz & Magleby (1986).

Simulation of channel currents. Single-channel currents were simulated according to the kinetic model given in scheme 1. The time spent in each state and transitions between states were calculated from the rate constants by methods similar to those described by Blatz & Magleby, 1986. Each dwell time was truncated to the nearest integer multiple of the simulated sampling interval, 6·25 μs. Gaussian noise was simulated by adding normally distributed, pseudo-random numbers to the simulated current record (subroutine GGEXN, International Mathematics and Statistics Library, Houston, TX, U.S.A.). In order to provide non-zero settling times, the simulated data was filtered (Gaussian FIR filter, −3 db at 20 kHz) and decimated by a factor of four, i.e. the mean amplitudes of groups of four data points were computed so that the final simulated sampling interval was 25 μs. Finally, the bandwidth was further limited by invoking the Gaussian filter during the single-channel-detection program. Thus the simulted data sets resembled the real data sets with regard to sampling rate (40 kHz), bandwidth (5 kHz), and signal-to-noise ratio.

RESULTS

General description of the single-channel currents

The following kinetic scheme will serve as the basis for our analysis of single-cholinergic-channel currents:

$$2A + C \underset{k_{-1}}{\overset{2k_{+1}}{\rightleftharpoons}} A + AC \underset{2k_{-2}}{\overset{k_{+2}}{\rightleftharpoons}} A_2C \underset{\alpha}{\overset{\beta}{\rightleftharpoons}} A_2O, \qquad \text{scheme 1}$$

where A is an ACh molecule, C is a closed receptor–channel, and O is an open receptor–channel. This scheme describes only the essential features of channel activation; sojourns in other open or closed states not associated with binding or gating are also possible (Jackson, 1984; Auerbach & Sachs, 1984; Sine & Steinbach, 1986).

In all preparations where it has been examined, currents from both large- and small-conductance cholinergic channels occur in bursts at all concentrations of ACh, i.e. more than one exponential is required to describe the distribution of closed intervals in a record. The association of intraburst intervals with states in the above kinetic scheme, however, depends on the concentration of ACh in the patch pipette. At low concentrations (40–200 nM), closed intervals are described by two to three exponentials and bursts largely reflect sojourns in open and closed doubly liganded states (Nelson & Sachs, 1979; Colquhoun & Sakmann, 1981, 1985). At high concentrations (2–200 μM), four to seven exponentials are required to describe the unconditional closed interval distribution and bursts largely reflect sojourns in the entire set of activatable states (regardless of ligation or gating state) plus shorter-lived desensitized states (Sakmann, Patlak & Neher, 1980; Sine & Steinbach, 1987).

In *Xenopus* myocytes channels are heterogeneous both with regard to conductance and kinetics and it is therefore difficult to describe in detail the complete kinetic architecture of bursts for a single population of channels. We do not as yet know whether the kinetic heterogeneity reflects different behaviours of the same channel or the behaviour of distinct molecular forms of the channel. In the present experiments using high ACh concentrations, bursts were defined (see Methods) to isolate intervals associated with the activatable states of a single kinetic class of channel –

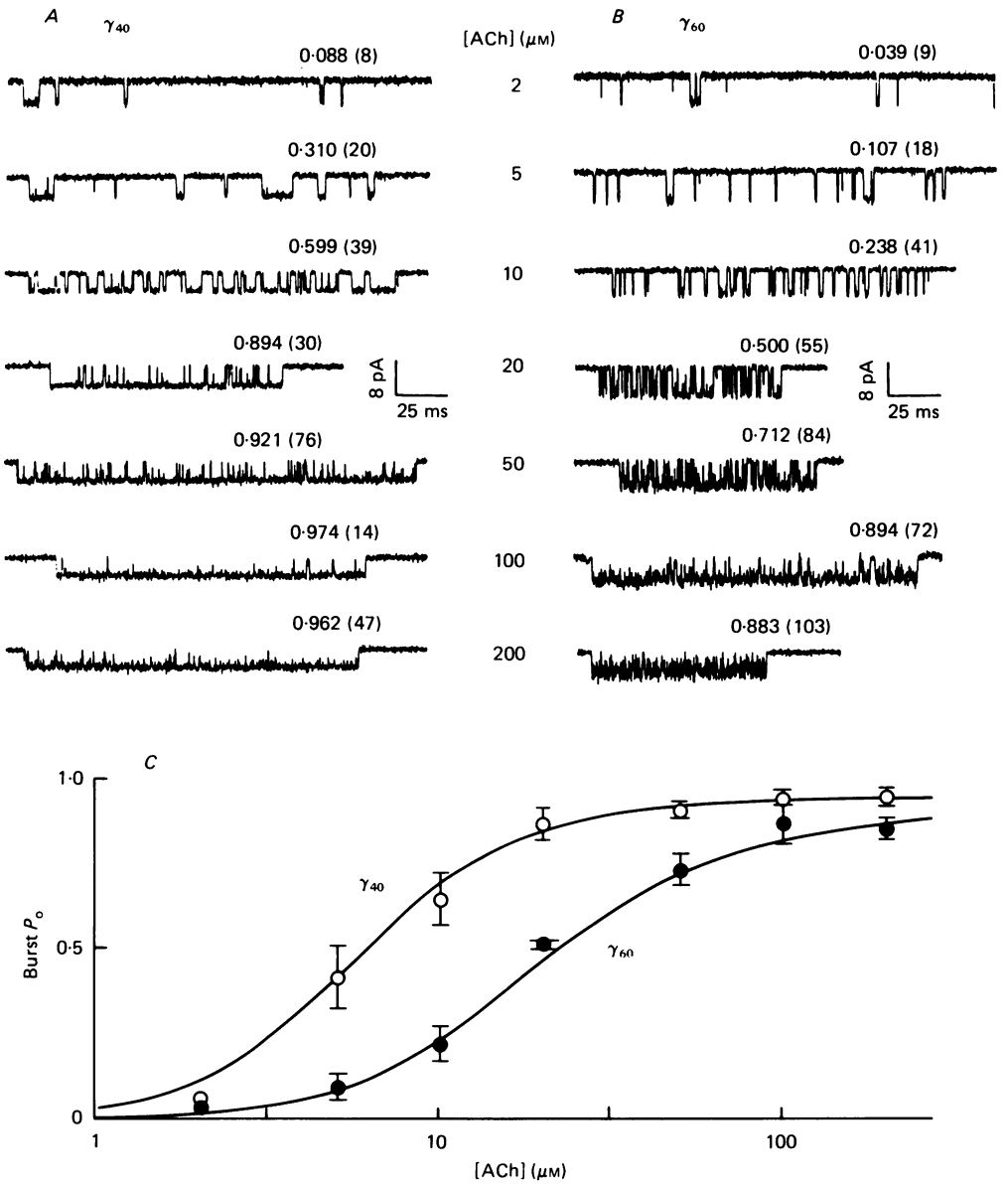

Fig. 1. *A* and *B*, examples of γ_{40} and γ_{60} H-mode bursts at various ACh concentrations. The γ_{40} trace at 2 and 5 μM-ACh reveal only portions of bursts. The probability of being open (P_o) and number of openings (given in parentheses) are indicated above each burst. Data are from cell-attached patches, estimated membrane potential = −117 mV, 23–26 °C. *C*, P_o values *vs.* [ACh]. Data are expressed as mean ± S.D. (two to seven patches at each [ACh], nine to 225 bursts from each patch). Continuous lines are calculated from the rate constants in Table 3 (binding equivalence for γ_{60} channels, positive co-operativity for γ_{40} channels).

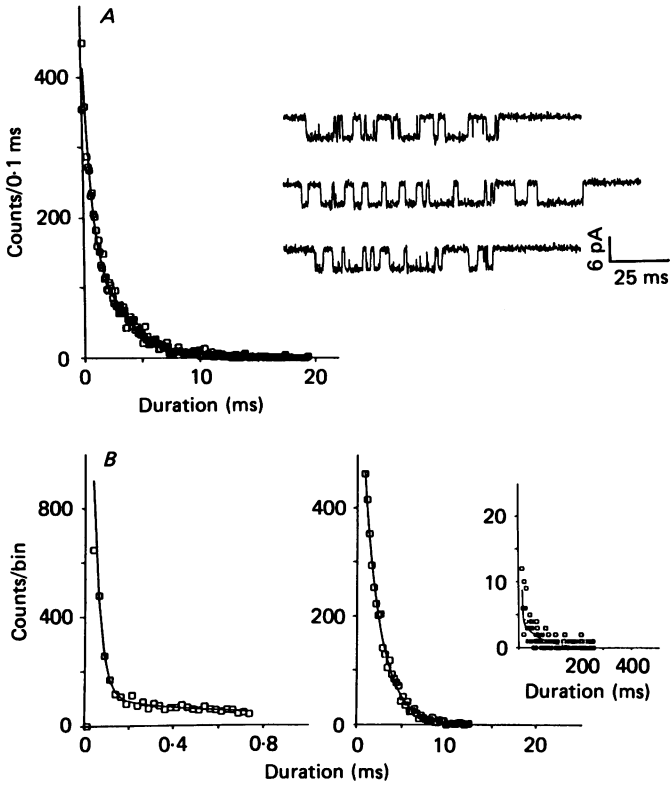

Fig. 2. Interval duration histograms and sample bursts for γ_{40} channels at 10 μM-ACh. Data taken from one patch; the time constants and relative proportions of each component are given in Table 1. *A*, open interval distribution, fitted by the sum of two exponentials. *B*, closed interval distribution, fitted by the sum of four exponentials. The slowest component had an apparent time constant of 66 ms (127 events, or 1·3% of all closed intervals). Closed intervals < 10 ms were defined as being within a burst. Single-channel current was 4·71 pA.

those with a high probability of being open (H-mode bursts). Previous work indicates that H-mode bursts represent the predominant kinetic behaviour of ACh channels under the particular parameters of our cultures; in general, a minimum of 85% of all bursts appear to have H-mode activity (Auerbach & Lingle, 1986*b*).

Examples of H-mode bursts elicited by a wide range of ACh concentrations are shown in Fig. 1. In the range 2–100 μM-ACh, the probability of being open within a burst (P_o) increases with increasing ACh for both large-conductance (γ_{60}) and small-conductance (γ_{40}) channels as expected from the decreasing residence of channels in vacant and monoliganded states.

Two conclusions can be drawn from the burst P_o *vs.* [ACh] data shown in Fig. 1*C*. First, at high [ACh], where according to scheme 1 P_o approaches $\beta/(\beta+\alpha)$, the observed P_o values are close to 1. This indicates that $\beta \gg \alpha$ for both conductance forms of channel. At 100 μM-ACh, the γ_{40} and γ_{60} P_o values are $0{\cdot}94 \pm 0{\cdot}04$ (mean $\pm$ S.D., $n = 4$) and $0{\cdot}86 \pm 0{\cdot}06$ ($n = 4$); if we let α equal the inverse of the open-interval duration (corrected for missed events and channel block; Fig. 6), we estimate

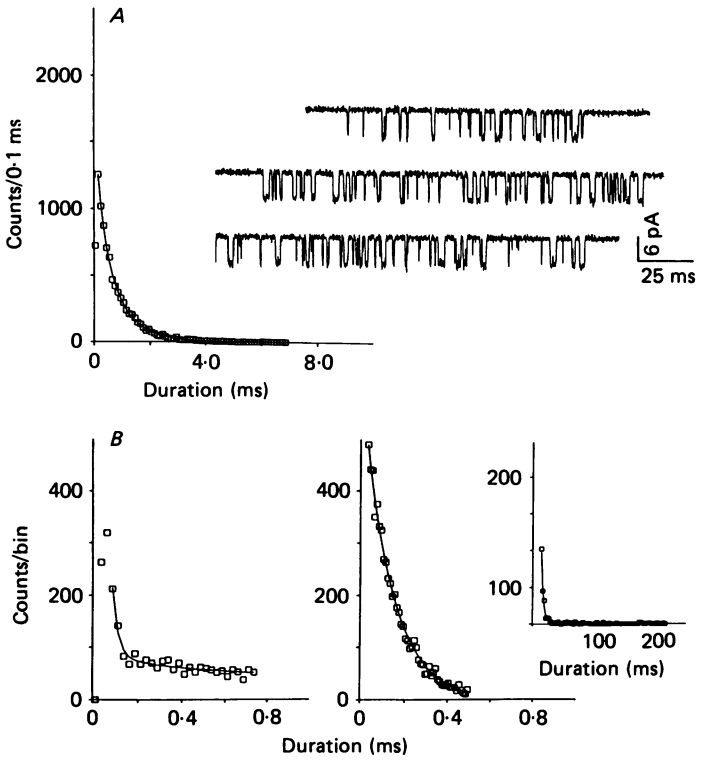

Fig. 3. Interval duration histograms and sample bursts for γ_{60} channels at 10 μM-ACh. Data taken from same patch shown in Fig. 2; the time constants and relative proportions of each component are given in Table 1. *A*, open interval distribution, fitted by the sum of two exponentials. *B*, closed interval distribution, fitted by the sum of four exponentials. The slowest component had an apparent time constant of 68 ms ($n = 83$, or 0·6% of the total). Closed intervals < 12 ms were defined as being within a burst. Single-channel current was 6·26 pA.

that β is > 5000 s^{-1} for γ_{40} channels and > 8100 s^{-1} for γ_{60} channels. These estimates are lower limits because the entry of channels into closed states not associated with the channel activation sequence reduces the observed P_o values. A second obvious feature of the P_o *vs.* [ACh] data is that the γ_{60} P_o values are shifted toward higher [ACh] relative to the γ_{40} P_o values. This indicates that the apparent equilibrium dissociation constant for the activation process, which is equal to the [ACh] at which P_o is half of its maximum value, is higher for γ_{60} channels (~ 25 μM) than for γ_{40} channels (~ 5 μM). While these observations set limits on the rate constants of channel activation, more quantitative estimates of the binding and gating rate constants can be obtained from analyses of open and closed interval durations within bursts as a function of [ACh].

General description of interval duration distributions

Some of the salient features of intraburst open and closed interval distributions can be seen in Fig. 2 (γ_{40} channels) and Fig. 3 (γ_{60} channels). The data shown are from one patch where [ACh] was 10 μM; the interval distribution parameters for this patch

are given in the left panel of Table 1. This data set is typical of γ_{40} and γ_{60} channel kinetics at all ACh concentrations in that open intervals are described by the sum of two exponentials and closed intervals are described by the sum of two or three exponentials. Variations on this general pattern are discussed in detail in later sections.

Our analysis focuses on the amplitudes and time constants of three kinetic components: slow open intervals, and fast and slow closed intervals. As a rule, in each patch the error limits on the estimates of these parameters were small. One exception was the accuracy of the estimate of the number of fast closures. Often the confidence limits on this parameter were very large because the time constant of this component (~ 40 μs) was similar to the system dead time (35 μs) and sampling interval (25 μs). The estimate of number of fast closures is used in the correction for missed events (see Methods), and the lack of precision of this parameter increases the scatter in the corrected interval durations.

The range of values obtained from six patches at 10 μM-ACh are given in the right panel of Table 1. For γ_{40} channels, 92% of open intervals were from the slow component ($\tau = 2{\cdot}46$ ms) and 58% of closed intervals were from the slow component ($\tau = 1{\cdot}95$ ms). A third component of closed interval distribution was present in only about half of the patches at 10 μM-ACh where it had a time constant (τ_{med}) in the range 0·4–1·4 ms and usually accounted for < 10% of all intraburst closed intervals.

The makeup of γ_{60}channel interval distributions was similar to that of γ_{40} channels with two exceptions. First, in many patches a single exponential was sufficient to describe the open interval durations. Second, although a fast component to the closed interval duration was always present, in many records it was too small and/or too fast to be accurately fitted.

Tests for homogeneity and stationarity

For a kinetic analysis to be meaningful the kinetic properties of the channels should be homogeneous for each patch. We attempted to ensure homogeneity by selecting bursts which had similar P_o values, but this parameter is a poor discriminator of kinetic behaviour because it is determined by a ratio of rate constants, and because it only weakly depends on [ACh] at both high and low ACh concentrations. Thus, at extremes of [ACh] it is difficult to distinguish between kinetic modes on the basis of the P_o statistic.

We gained some measure of kinetic homogeneity by computing the mean open or closed interval duration for each selected burst in a patch, and by comparing the variance of these means to that expected from a simple two-state kinetic model. The bandwidth of the data was limited to 2·6 kHz so that the computed mean values primarily reflect the slow component of the closed or open interval distributions (see Figs 2 and 3). Sums of k independent and identically distributed exponential random variables have a γ-distribution; the variance of this distribution changes with k, thus the scatter of the mean durations computed for each burst about the global mean will depend on the number of intervals in the burst.

Figure 4 is a plot of the mean open and closed interval durations *vs.* the number of events for each selected burst in a record. For a homogeneous, exponentially distributed population of intervals, 95% of the values should fall between the continuous lines, which have been computed from the one-parameter γ-distribution.

In the record shown, 85% of the mean open durations and 76% of the mean closed durations fall within these limits. In eight patches where such an analysis was made (2–50 μM-ACh, γ_{40} and γ_{60} bursts), 83% of mean open interval durations and 82% of mean closed interval durations fell within the 95% limits. Bursts which had mean interval durations outside the limits were equally distributed below and above the lines.

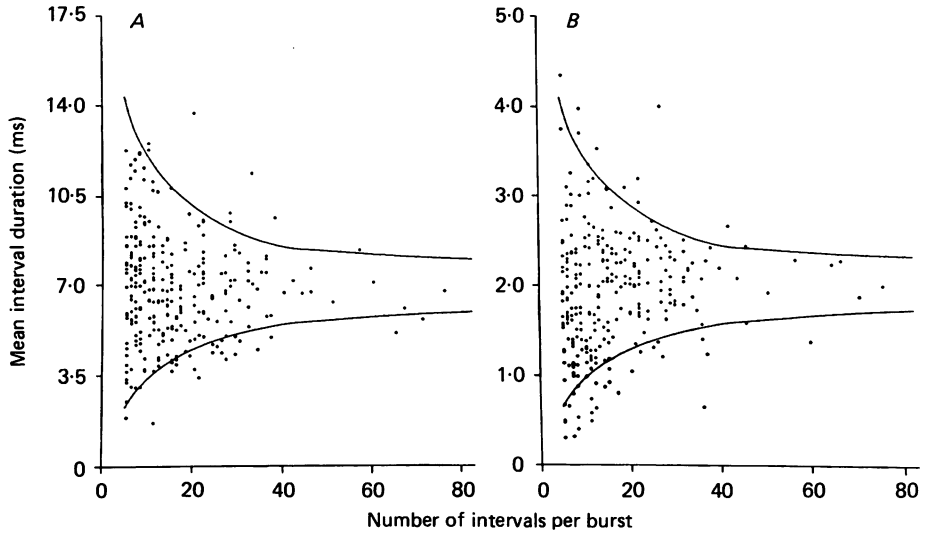

Fig. 4. Homogeneity of burst kinetic parameters. Mean burst open interval durations (*A*) and mean burst closed interval durations (*B*) plotted as a function of the number of openings in the burst. Each point represents one burst; if open–closed interval durations were described by a single exponential, 95% of the points should fall between the continuous lines. γ_{40} bursts at 50 μM-ACh.

The above analysis assumes that intervals are distributed as a single exponential when in fact both open and closed interval distributions have multiple components. Thus scatter greater than that predicted by the one-parameter γ-distribution is expected. The data suggest that in high [ACh] experiments, most of the bursts we selected for kinetic analysis are homogeneous with regard to the predominant (slow) components of open and closed intervals. Whether or not all of the excess variance in the data can be attributed to the over-simplified model is problematical, and it is likely that our analysis included some bursts which had kinetic properties different from the main population. Also, we have not tested for kinetic homogeneity in low [ACh] experiments, although as indicated below some open interval distributions at low [ACh] contain an additional component which has been excluded from the analysis of the high-concentration records.

Another criterion for a meaningful kinetic analysis is that the kinetics in a given patch be stationary. To test for any time dependence of kinetic parameters, the mean open duration, mean closed duration, mean P_o, and mean burst amplitude were compiled for all selected H-mode γ_{40} bursts in a record and were plotted as a function of time (Fig. 5). The bandwidth was 2·6 kHz.

At high [ACh], for $\sim$ 30 s after the start of data recording the mean burst amplitude often increased, presumably due to the recovery of the membrane potential following

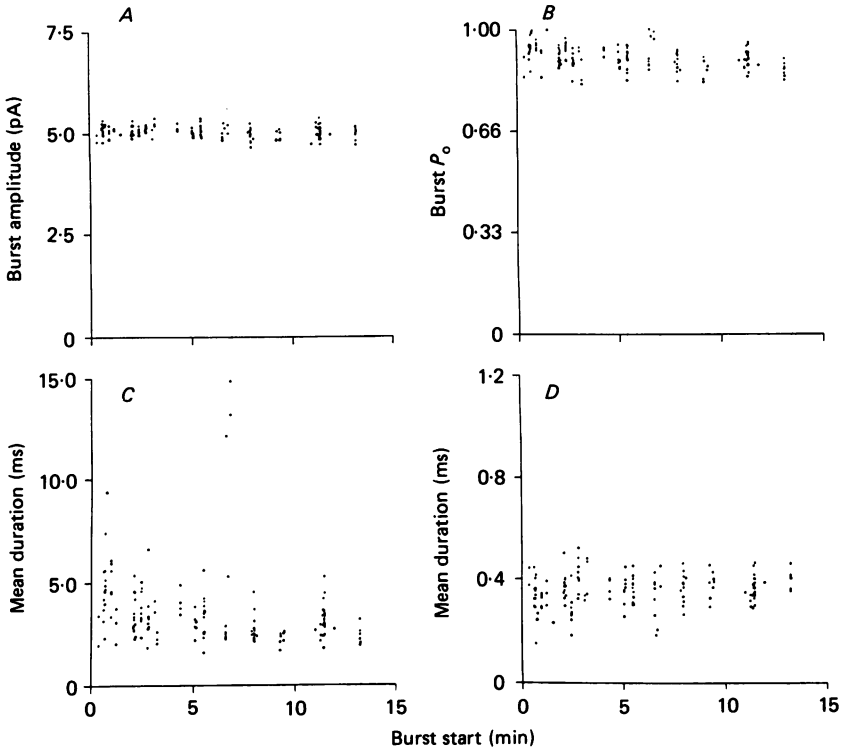

Fig. 5. Stationarity of kinetic and amplitude parameters. For each selected burst in the record, the mean open interval amplitude (*A*), probability of being open (*B*), mean open intervals duration (*C*) and mean closed interval duration (*D*) are plotted as a function of time after the start of data recording (20 μM-ACh; γ_{40} channels). There is some drift in the mean open interval duration of bursts.

the exposure of the whole cell to agonist during the approach of the patch pipette. The extent of the calculated repolarization increase was small, < 10 mV. A second parameter which occasionally showed time dependence was the mean open interval duration. In about half of the patches it decreased with time, resulting in a concomitant decrease in the burst P_o. At high [ACh], the drift in mean open duration, which could be as much as 20% of the steady-state value, occurred over a period of several minutes (see Fig. 5*C*).

In all patches which were examined, the mean closed interval durations did not exhibit any significant time dependence. We conclude that the kinetic processes underlying the predominant, slow component of closed intervals within bursts are stationary over our recording period, 0·5–30 min after seal formation. The kinetics of open intervals, however, are less static. Therefore, our estimates of this parameter for γ_{40} channels are likely to be weighted averages of mean interval duration of all openings in a patch.

To estimate activation rate constants it was necessary to combine data from many patches exposed to many concentrations of ACh. Consequently, two additional criteria for our analysis are that patch-to-patch variability of kinetic parameters be moderate, and that the rate constants of the model be independent of [ACh]. The

scatter in the estimated kinetic parameters at the same [ACh] can be seen in Tables 1 and 2. Before correcting for missed events, the key kinetic parameters for our analysis – the time constants of the main component of open and closed interval durations – varied by $< 15\%$ of the mean values for γ_{40} channels. The scatter in these parameters for γ_{60} channels was somewhat larger but still was $< 35\%$ of the means. These variations are moderate when compared to the more than 100-fold change in kinetics which take place as the [ACh] varies (see Fig. 9).

We have not tested if the rate constants and/or underlying kinetic scheme change with [ACh].

To summarize, analyses of a few patches indicates that as a first approximation, the two criteria of homogeneity and stationarity are satisfied for intraburst closed intervals at high [ACh]. However, this conclusion must be tempered because only a limited number of files were analysed, and because in these tests the scatter in interval duration means rather than distributions were measured. We therefore cannot eliminate the possibility that the kinetic parameters we measure reflect the mean behaviour of a population of non-identical channels, i.e. either distinct classes of proteins and/or a single class with time-varying kinetic properties.

Identity of closed intervals

There are three closed states in the basic activation sequence (scheme 1). If bursts at high ACh concentrations represent channels in activatable states then the unconditional closed interval distribution of bursts should have three exponential components with time constants and amplitudes given by Colquhoun & Hawkes (1981). Many cholinergic channels can enter short-lived states which apparently are not associated with channel activation (Auerbach & Sachs, 1984; Sine & Steinbach, 1984; Colquhoun & Sakmann, 1985), and it is important to identify which of the three components we observe in the intraburst closed interval distributions are involved in the primary activation sequence of the ACh channel.

The time constant of the slowest component of the closed interval duration distribution ($\sim 60\%$ of all intraburst gaps at 10 μM-ACh), becomes shorter with increasing [ACh] (see Fig. 9) and thus can reasonably be associated with ACh binding and channel activation. This criterion cannot be used as identification of the fastest and intermediate closed interval components (~ 35 and $\sim 5\%$ of all intraburst gaps at 10 μM-ACh, respectively) because both the time constants and relative fraction of these components show little dependence on [ACh]. We have not determined if some fraction of fast or intermediate gaps are partial closures, or if the durations of these events depend on the nature of the agonist. Therefore we have no clear evidence either negating or supporting the supposition that fast and/or intermediate closures reflect one or more steps in the channel activation process.

The association of fast and/or intermediate gaps with states of the model can be guided by the observation that P_0 values at high [ACh] are close to 1. At limiting low [ACh], gaps which reflect sojourns in the A_2C state have a time constant (τ_{gap}) equal to $1/(\beta+2k_{-2})$ and occur with a relative frequency (n_{gap}, or the number of gaps per burst) determined by $\beta/2k_{-2}$(Colquhoun & Hawkes, 1977). The magnitude of β thus sets limits on the expected characteristics of gaps at low [ACh]: if $\beta \gg k_{-2}$, τ_{gap} would approach its maximal value ($< 0{\cdot}2$ ms for γ_{40} channels) and n_{gap} would be large.

In our experiments with γ_{40} channels, at 100 nM-ACh $\tau_{med} = 0{\cdot}75 \pm 0{\cdot}29$ ms and $n_{med} = 0{\cdot}12 \pm 0{\cdot}07$ (mean $\pm$ S.D., $n = 5$). Assuming α to be 350 s^{-1}, these parameters predict a maximum burst P_o of 0·29. This is clearly at odds with the observed P_o data (Fig. 1*C*), and we conclude that intermediate duration closures at low [ACh] are too slow and too rare to reflect sojourns in the doubly liganded, closed state of scheme 1. Under the same experimental conditions, τ_{fast} was $0{\cdot}042 \pm 0{\cdot}09$ ms and n_{fast} (the number of fast gaps per burst) was $0{\cdot}36 \pm 0{\cdot}18$ (see Table 2). These parameters predict a maximum burst P_o of 0·96, close to the observed value. The properties of fast closures are thus in accord with those expected from gaps representing sojourns in the A_2C state.

It is also not likely that the observed population of intermediate closures represents the intermediate duration closed interval component predicted by the four-state model. The model predicts that relative fraction of events from the intermediate component should vanish both at low and high [ACh], while in our experiments the fraction of intermediate events was independent of [ACh]. At 100 nM-ACh, intermediate closures constituted $8 \pm 4\%$ ($n = 6$) of all closed intervals in the record, identical to the value at 10 μM-ACh (Table 1). Moreover, both the relative occurrence and time constant of intermediate closures varied considerably from patch-to-patch at each [ACh]. We therefore conclude that intermediate closures do not pertain to the main activation sequence of scheme 1.

In general, the time constant of intermediate closures allows clear separation from other components of interest. However, τ_{slow} is in the same range as τ_{med} at ~ 20 μM-ACh for γ_{40} channels and at ~ 50 μM for γ_{60} channels. Under these conditions, a separation of intermediate closures from the primary, [ACh]-dependent (τ_{slow}) component is not usually possible. As such, this component, although minor, may in some cases contribute inaccuracy in the estimates of the amplitude and time constant of other components. Intermediate closures will not be considered further here.

Kinetic parameters at low [ACh]

At low [ACh] (40, 100 and 200 nM), bursts were defined as groups of openings separated by closed intervals less than 2 or 3 ms. Open interval, closed interval and burst durations were examined at low [ACh] in sixteen patches for γ_{40} channels and thirteen patches for γ_{60} channels (Table 2). Assuming that all fast closures represent sojourns in the doubly liganded, closed state of the channel, the duration of fast closures and the number of fast closures per burst can be used to calculate β and k_{-2} (Colquhoun & Hawkes, 1977). We will use these estimates as the starting point of our analysis.

Since bursts elicited by low [ACh] were selected for analysis solely on the basis of amplitude kinetic homogeneity of the data could not be assured. Indeed, in seven of the sixteen γ_{40} patches, open interval distributions had a third component in the range 1·0–1·5 ms which accounted for 5–30% of the total. We suspect that these currents are from γ_{40} channels which have kinetic properties distinct from the main population of channels because their time constant and relative fraction of occurrence were similar to M-mode cholinergic channels (Auerbach & Lingle, 1986*b*), and because such an open interval component is not present in the selected H-mode bursts at high [ACh]. We have excluded this component from the analysis of open interval and burst durations at low [ACh].

In a given patch, the burst durations paralleled those of open intervals with regard to the number, proportions and relative magnitude of the time constants of the distribution (Fig. 6 and Table 3). For γ_{40} currents at low [ACh], the duration of fast intraburst closures was $0{\cdot}041 \pm 0{\cdot}016$ ms (mean $\pm$ S.D.). The most reliable estimate of the number of openings per burst was the ratio of the open interval duration main component (corrected for missed closures) to the burst duration main component and was equal to $1{\cdot}40 \pm 0{\cdot}22$ for γ_{40} channels. These values yield estimates of 7040 s^{-1} for β and 8800 s^{-1} for k_{-2}.

There are two main sources of error in these estimates. First, open interval durations are usually distributed as the sum of two exponentials and the proportion of fast closures which occur during slow openings only is not known. The missed event correction, however, assumes that all fast closures occur during slow open intervals. Thus the corrected open interval durations are underestimated and the number of openings per burst are overestimated. The second source of error stems from the fact that the time constant of fast closures is similar to the system dead time, sampling interval and histogram bin width. As a consequence, the estimated number of events from this component are imprecise and are biased towards larger values (Sine & Steinbach, 1986). Again, this would tend to underestimate the true open interval duration and overestimate the number of openings per burst. Thus, the estimates of β and k_{-2} given above should be considered upper and lower limits, respectively.

A similar kinetic analysis for γ_{60} channels at low [ACh] is not possible because in most files the number of detected fast closures was too small to quantify. We therefore combined open, closed and burst interval duration histograms from thirteen patches in order to estimate the durations and number of these events (Table 2). In these files, the mean duration of fast closures was 0·023 ms and the mean number of openings per burst (after correcting for missed events) was 1·53. From these values we estimate that $\beta = 17\,100\,s^{-1}$ and $k_{-2} = 13\,100\ s^{-1}$. These values are not very precise and should only be taken as rough estimates because the error limits on both the mean duration and number of fast gaps were rather large, and because the missed events correction was applied to a data set combined from many patches.

Open interval parameters vs. [ACh]

Figures 6 and 7 show the time constants and relative proportions of the fast and slow components of open interval distributions as a function of [ACh] for γ_{40} and γ_{60} channels. Between 40 nM and 20 μM (over a 500-fold range in [ACh]) there was essentially no change in any of the three parameters associated with open intervals. The singular independence of these parameters on [ACh] is predicted by the basic activation scheme and suggests that in *Xenopus* myocytes most fast open intervals within bursts represent doubly rather than singly liganded channels; if monoliganded channels opened briefly, the relative frequency of fast open intervals would be expected to decrease with increasing [ACh].

For both conductance forms of channels, τ_{slow} for open intervals decreases at concentrations of ACh $> 20\ \mu$M. This decrease is consistent with the idea that ACh molecules block open nicotinic channels (Sine & Steinbach, 1984; Ogden & Colquhoun, 1985). The curves in Fig. 6 were fitted to the data according to a standard sequential model for channel block:

$$\tau_{open,\,slow} = (\alpha + f[ACh])^{-1},$$

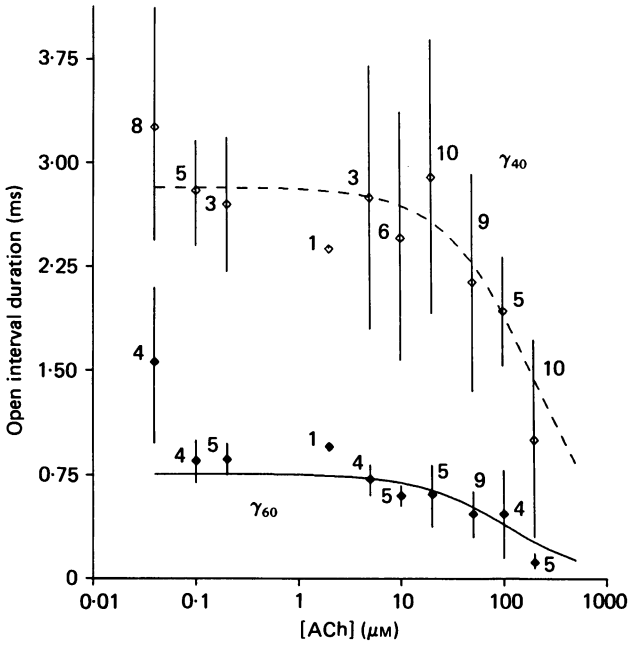

Fig. 6. Open interval durations as a function of [ACh]. Open symbols and dashed line, γ_{40} channels; closed symbols and continuous line, γ_{60} channels. The data have been corrected for missed events (see Methods). The lines are drawn according to a linear channel blocking model. Bars indicated $\pm$S.D.; the numbers indicated the number of patches at each [ACh].

where f is the forward rate of channel block. From these data we estimate apparent channel closing rates (α) of 354 ± 19 s^{-1} for γ_{40} channels and 1320 ± 149 s^{-1} for γ_{60} channels. These estimates are similar to those reported previously (Brehm, Kidikoro & Moody-Corbett, 1984). We also estimate the forward rate of channel block by ACh to be $3{\cdot}0 \pm 0{\cdot}5 \times 10^6$ M^{-1} s^{-1} for γ_{40} channels and $3{\cdot}5 \pm 0{\cdot}3 \times 10^7$ M^{-1} s^{-1} for γ_{60} channels. These values are comparable to those reported from ACh block of cholinergic channels in BC_3H1 cells (Sine & Steinbach, 1984) and the adult frog end-plate (Ogden & Colquhoun, 1985) and *Xenopus* myocytes (Igusa & Kidokoro, 1987).

For γ_{40} channels, the fast component of the open interval duration distributions was consistently observed ($\sim 20\%$ of the total) and had a time constant of 200–500 μs (Fig. 7). For γ_{60} channels, a fast component of open intervals could be detected in about one-third of the patches. It is not certain that the lack of detected fast openings in γ_{60} channels is due to their faster time constant: in those patches where a fast component was present, the time constant was ~ 160 μs, well above the detection limit of the system.

Closed interval parameters vs. [ACh]

The concentration dependence of the kinetics of closed intervals within bursts was quantified between 2–100 μM [ACh]. For each file three kinetic parameters were measured: the time constants of the slow and fast components of the distributions and the fraction of closures which belonged to the fast component.

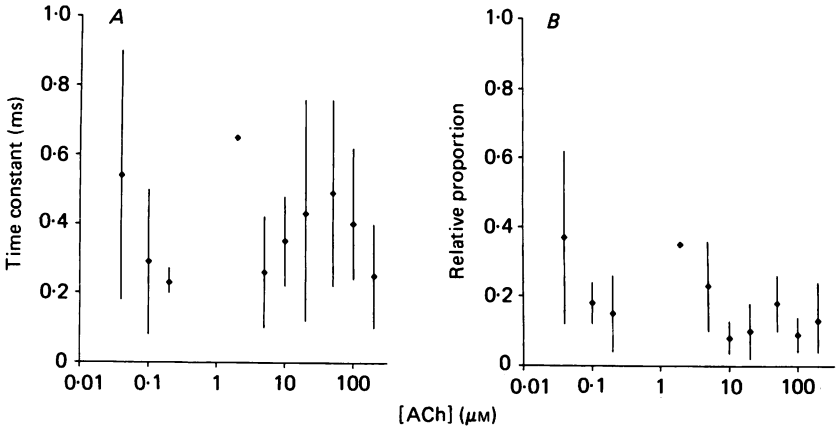

Fig. 7. Characteristics of short open intervals within bursts for γ_{40} channels. The time constant (*A*) and relative proportion (*B*) of short openings are plotted as a function of [ACh]. There is no significant trend in either parameter between 40 nM and 200 μM-ACh. Error bars are ±S.D.

Only a limited range of [ACh] could be examined. At concentrations below ~ 2 μM burst P_o values were very low and the probability of analysing bursts where more than one channel contributed currents was high enough to bias the closed interval distributions (Jackson, 1984; Sine & Steinbach, 1986). At [ACh] above ~ 100 μM, fast closures due to channel block dominated the intraburst closed interval distribution, and the components of closures arising from binding and gating become difficult to accurately measure.

For γ_{40} channels, τ_{fast} varied little between 2–100 μM-ACh where it was 42 ± 13 μs (mean ± S.D., thirty patches; range = 37–48 μs) (Fig. 8). This value is similar to the observed τ_{fast} at low [ACh] (Table 2). For γ_{60} channels, τ_{fast} also did not vary with [ACh] but was slightly more variable ranging from 29–48 μs over the same spread of [ACh].

Figure 8 also shows that for γ_{40} channels the relative fraction of events from the fast component of intraburst closed intervals (f_{fast}) increases with increasing [ACh]. Although some of the fast closures at high [ACh] reflect channel block by ACh molecules, it is not certain that all of the excess can be attributed to blockade because the channel blocking rate given above predicts that the relative proportion of blocking gaps should increase more gradually than actually observed.

The predominant component of the closed interval duration distributions, τ_{slow}, shows a strong dependence on [ACh] (see Fig. 1). Since this parameter reflects the total time a channel spends in the set of closed, activatable states, we will focus our analysis on its inverse, β', the effective channel opening rate. It should be emphasized that β' bears no simple relationship to any of the microscopic rate constants in the activation scheme.

For both conductance forms of channel, β' increases over 100-fold as the [ACh] increases from 2 to 100 μM (Fig. 9). Two major differences between γ_{40} channels and γ_{60} channels are apparent. (1) In the range of [ACh] examined, β' values saturate for

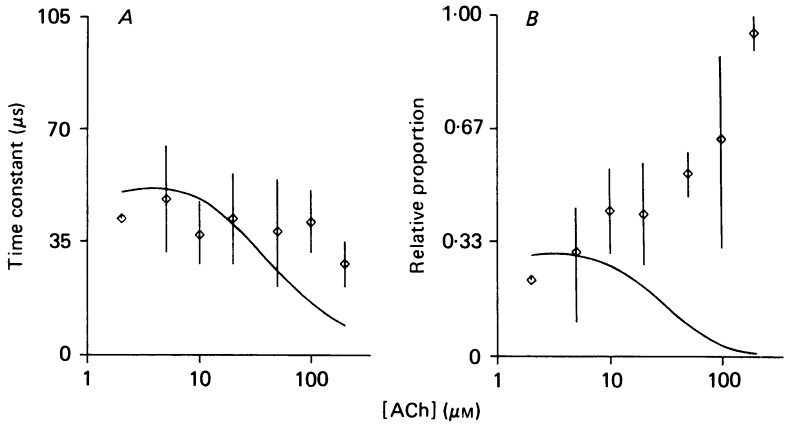

Fig. 8. Characteristics of fast closed intervals within bursts for γ_{40} channels. The time constant (*A*) and relative proportion (*B*) of fast closures are shown as a function of [ACh]. The time constant does not change significantly between 2 and 200 μM; the relative proportion increases with increasing [ACh], in part because of channel block by agonist molecules. The error bars are $\pm$S.D.; the continuous curves are calculated from the rate constants in Table 3 (column 2) and represent fast closed intervals expected from a combination of the two fastest eigenvalues predicted by the four-state model (scheme 1).

γ_{40} channels but do not for γ_{60} channels. (2) At [ACh] below 50 μM, β' values for γ_{40} channels are greater than for γ_{60} channels. From these two observations we can make the qualitative conclusions that the effective channel opening rate for γ_{40} channels is less than that for γ_{60} channels, and that γ_{40} channels have a higher affinity for ACh than do γ_{60} channels.

Estimating activation rate constants

In our data, only two components of the closed interval duration histograms are potentially associated with the activation process. One possible basis for this discrepancy between the prediction of the model and the observed results is that the activation sequence as given is too complex and there are only two closed, activatable states. This hypothesis is unlikely because the saturation of β' at high [ACh] indicates that for γ_{40} channels an agonist-independent conformational change is necessary for channel gating (one closed state), and many studies have shown that open cholinergic channels usually have at least two agonist molecules bound (two or more additional closed states). A more likely reason for the apparently missing kinetic component is that the specific values of the activation rate constants are such that only two components are apparent under the experimental conditions. This could occur because (1) the relative fraction of events from one component is too small, (2) the time constant of one component is too fast, and/or (3) the time constant of one component is too similar to that of another component to be resolved.

Since the observed closed interval parameters at any one [ACh] are insufficient to estimate activation rates, we have attempted to uncover a set or sets of rate constants which are consistent with our data at all ACh concentrations. Specifically, three aspects of the data need to be explained: (1) the time constants and frequency of occurrence of fast closures at low [ACh] (Table 2), (2) time constant and relative

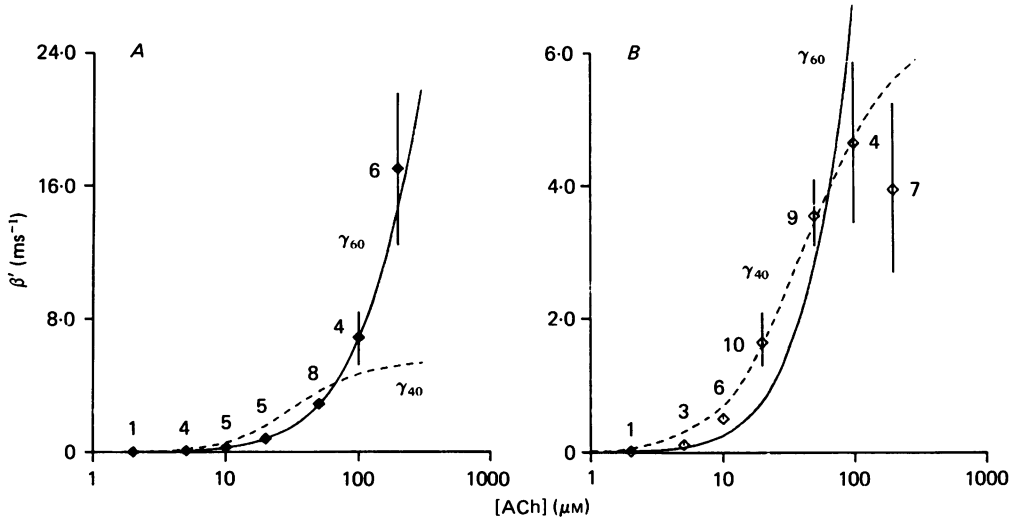

Fig. 9. The effective channel opening rate (β') as a function of [ACh]. The filled symbols represent γ_{60} channels; the open symbols represent γ_{40}channels. The lines (continuous, γ_{60}; dashed, γ_{40}) are calculated from the rates given in Table 3. Note the difference in scale between left and right panels. Error bars are ±S.D. and are less than the symbol height at some ACh concentrations; the number of patches is indicated near each symbol.

proportion of fast closures at high [ACh] (Fig. 8), and most critically, (3) the dependence of β' on [ACh] (Fig. 9).

Rate constants and data were compared in two stages. First, the equations given in Colquhoun & Hawkes (1981) which describe the unconditional distribution of intraburst closures were used to fit the β' *vs.* [ACh] curves in the range 2–100 μM (the 200 μM data were excluded because of contaminating gaps arising from channel block). Second, the rate constants so obtained were used to compute the expected relative amplitudes (assuming a 35 μs dead time) and time constants of each of the three components to the closed-interval distributions between 40 nM and 200 μM-ACh which are predicted by the standard activation scheme.

For many sets of rate constants, the computed values of the two fastest components of the closed interval distribution were such that they would not have been resolved as two components during the histogram fitting procedure of our experimental data (e.g. had time constants of 40 and 60 μs). Therefore, we also combined the two fastest closed interval components by weighting the time constant of each by the probability of an event from that population occurring. In this way the three closed interval components predicted from scheme 1 were fused into two.

The β' *vs.* [ACh] data were fitted under three conditions. First, k_{-2} and β were fixed at their values calculated from the low-concentration data (Table 2), and the data were fitted assuming that the microscopic rates of ACh association and dissociation are identical for the first and second binding steps (binding equivalence). Under these conditions, only one parameter, k_{+1}, was determined from the fit. Second, the assumption of binding equivalence was maintained but all three rate constants (k_{+1},

TABLE 3. Estimates of activation rate constants

Binding constraints:	Equivalence	Equivalence	Non-equivalence possible
Fitting constraints:	(β, k_{-2} fixed)	(No fixed rates)	(No fixed rates)
γ_{40} k_{+1} ($\times 10^8$)	4·8	5·1	6·2
k_{-1} ($\times 10^3$)	8·8	8·1	40·8
k_{+2} ($\times 10^8$)			9·4
k_{-2} ($\times 10^3$)			6·7
β ($\times 10^3$)	7·0	6·6	5·6
α	341	346	349
Sum squares ($\times 10^{-3}$)	16·3	13·3	2·3
$K_{d,1}$ (μM)	18·1	16·5	65·5
$K_{d,2}$ (μM)			7·1
γ_{60} k_{+1} ($\times 10^8$)	2·9	1·3	1·2
k_{-1} ($\times 10^3$)	13·1	6·1	5·1
k_{+2} ($\times 10^8$)			1·1
k_{-2} ($\times 10^3$)			6·5
β ($\times 10^3$)	17·1	38·2	56·3
α	1520	3960	5150
Sum squares ($\times 10^{-4}$)	470	0·6	0·3
$K_{d,1}$ (μM)	45·8	48·4	43·8
$K_{d,2}$ (μM)			57·3

All rates are in units of s^{-1} or $M^{-1}s^{-1}$ on a per site basis. Curves drawn according to some of these sets of rates are shown in Figs 9–11. The α estimates have been calculated from the burst duration at low [ACh] (Table 2) and the other rate constant estimates. $K_{d,1}$ and $K_{d,2}$ are equilibrium dissociation constants.

k_{-1} and β) were allowed to vary. The values from the first fitting procedure were used as seed values and the convergence criteria were relaxed in order to find a local minimum in the sum of squares. Third, the constraint of binding equivalence was removed and the data were fitted by a model where all five rate constants (k_{+1}, k_{-1}, k_{+2}, k_{-2} and β) could vary. Again, the seed values were those obtained by the previous method of fitting the β' data.

The rate constant estimates obtained under each of these conditions are shown in Table 3. Two clear differences between γ_{40} and γ_{60} channels emerge with respect to the activation kinetic parameters. Regarding channel gating, the estimated microscopic channel opening rate, β' is more than 5 times faster for γ_{60} channels ($\sim 40000\ s^{-1}$) than for γ_{40} channels ($\sim 6000\ s^{-1}$). Regarding agonist affinity, under the conditions of equivalence in binding, the estimated microscopic equilibrium dissociation constant (K_d per site) is ~ 3 times higher for γ_{60} channels ($\sim 48\ \mu$M) than it is for γ_{40} channels ($\sim 16\ \mu$M). For both conductance forms of channel, the individual rate constants for ACh association and dissociation are in the ranges $1–5 \times 10^8\ s^{-1}\ M^{-1}$ and $5–9 \times 10^3\ s^{-1}$, respectively. However, the error limits on the estimated rates are quite large, and we cannot determine whether the affinity difference between γ_{60} and γ_{40} channel arises from differences in the agonist association or dissociation rates.

For γ_{40} channels, there is little difference in the estimated rates when β and k_- are fixed by low [ACh] results, and when β' k_-, k_+ are allowed to vary (equivalence in binding assumed). For γ_{60} channels, however, the rate constants obtained from the low-concentration data do not adequately describe the β' *vs.* [ACh] curve, as they underestimate β several-fold.

Relaxing the requirement for binding equivalence results in a better fit to the β' data for γ_{40} channels, with the equilibrium dissociation constant for the first binding step being $\sim$ 10 times lower than that for the second binding step (Table 3, column 3). While this suggests that ACh binding rates are not equivalent, we cannot conclude that the shape of the γ_{40} β' curve is strongly indicative of positive co-operativity in ACh binding; there are two extra degrees of freedom in the fit to all five rate constants and a better fit would be expected on this basis alone. For the γ_{60} β' data allowing all five activation rates to vary does not result in a better fit to the β' data set. Thus, unlike γ_{40} channels, there is no suggestion of positive co-operativity in ACh binding to γ_{60} channels.

TABLE 4. Some calculated and observed kinetic parameters

Binding constraints:	Equivalence	Non-equivalence possible	Observed
at 40 nM-ACh:			
$\tau_{closed,fast}$ (μs)	43	52	41
openings/burst	1·39	1·42	1·40*
openings/burst 5 kHz	1·17	1·21	1·20
maximum P_o:			
infinite bandwidth	0·95	0·94	
5 kHz bandwidth	0·98	0·97	>0·94
K_d (apparent) (μM)	4·7	6·0	~5
at 40 nM-ACh:			
$\tau_{closed,fast}$ (μs)	20	14	23
openings/burst	4·11	5·34	1·53*
openings/burst 5 kHz	1·54	1·27	1·18
maximum P_o:			
infinite bandwidth	0·91	0·91	
5 kHz bandwidth	0·99	0·99	>0·86
K_d (apparent) (μM)	23·1	22·7	~25

Calculated parameters obtained from rates given in Table 3 according to scheme 1 (channel block ignored). * Calculated using the missed events correction assuming a bandwidth of 5 kHz.

Predictions from the rate constant estimates

The rate constants in Table 3 (column 2) have been used to calculate kinetic parameters of currents (Table 4) and closed interval distribution time constants and amplitudes as a function of [ACh] (Fig. 10).

When fitting the experimentally determined interval duration histograms, components which are too fast (less than $\sim$ 35 μs), too rare (less than $\sim$ 5% of the total) and/or too similar to other components with regard to characteristic time constant are difficult to detect. Under our experimental conditions, the rates given in Table 3 (assuming binding equivalence) predict that for both conductance forms of channel only two components would be apparent in the intraburst closed interval duration histograms for all ACh concentrations for both γ_{40} and γ_{60} channels. Sometimes, the fastest component would be too fast to be measured; for γ_{60} channels at all ACh concentrations, the predicted time constant of the fastest closed interval component is $\leqslant 20$ μs. In other instances, a closed interval component would be too rare to detect; the predicted amplitude of the intermediate closed interval population for γ_{60} channels is $< 10\%$ of the total below 100 μM-ACh. Finally, under some

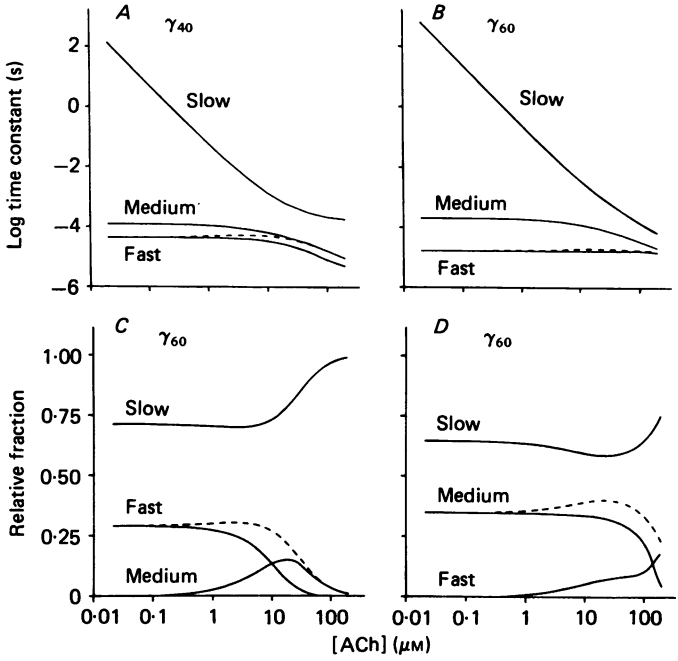

Fig. 10. Predicted closed interval duration distribution parameters as a function of [ACh]. The kinetic model is given in scheme 1; the rate constants are given in Table 3, column 2. *A* and *B*, time constants for γ_{40} and γ_{60} channels. *C* and *D*, relative amplitudes for γ_{40} and γ_{60} channels. Under our experimental conditions, the fast and medium components would merge (dashed lines).

conditions the two fastest time constants would be too similar to be separately resolved and would fuse into a single component; for γ_{40} currents at 10 μM-ACh a 34 and a 63 μs component would fuse to form one 49 μs component. Thus, even though the four-state activation scheme requires that intraburst closed interval durations be described by the sum of three exponentials, in our experiments only two of the three components are apparent because the bandwidth, the sampling interval and/or the number of measured intervals were limited.

The concentration dependence of the apparent component of closures which arises from a merger of the fast and medium components is shown as dashed lines in Fig. 10. A higher resolution view of this 'fused' component is shown for γ_{40} channels in Fig. 8. Over the range 5–50 μM-ACh, the predicted and experimentally observed time constants are in reasonable agreement. At higher [ACh], the predicted and observed values for time constant and relative proportion disagree; this is in part due to channel block by agonist molecules.

The rate constants and the observed burst durations at low [ACh] (Table 2) can be used to obtain an estimate of the true channel closing rate, α:

$$\tau_{\text{burst}} = (1/\alpha)\{1+[\beta/(2k_{-2})]\}+[1/(\beta+2k_{-2})](\beta/2k_{-2}).$$

For γ_{40} channels, there is an excellent agreement between the observed and predicted parameters concerning fast closed intervals. α calculated from the rates (346 s^{-1}

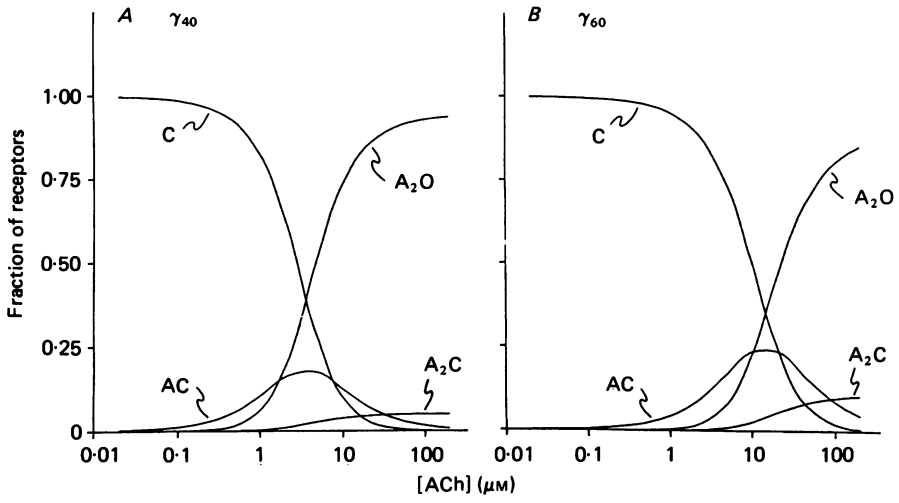

Fig. 11. Predicted steady-state occupancies of channels in activatable states. The kinetic model is given in scheme 1; the rate constants are given in Table 3, column 2.

assuming equivalence in binding; Table 3) agrees well with α estimated using the standard missed events correction (354 s^{-1}; see Fig. 6). Thus for γ_{40} channels, the inverse of the open-channel duration closely reflects the true channel closing rate. This is not the case for γ_{60} channels where the rates predict α to be 3960 s^{-1} (Table 3), 3 times faster than that obtained with the missed events correction (1320 s^{-1}; Fig. 6). We think that this discrepancy arises because fast closures of γ_{60} channel are too fast to be reliably detected and that in the analysis of low [ACh] results we overestimated their duration and underestimated their number. This in turn would lead to underestimates of β, the number of openings per burst, and the true channel closing rate.

The activation of γ_{60} channels is shifted toward higher [ACh] relative to γ_{40} channels (Fig. 1*C*). Figure 11 shows the steady-state occupancy of channels in each of the four states of the activation scheme as a function of [ACh], calculated from the rate constants of Table 3 (assuming binding equivalence; column 2). For a population of channels, the rates predict that at steady state, the concentration of ACh which opens half of the channels (the apparent equilibrium dissociation constant) is 24 μM for γ_{60} channels and 5 μM for γ_{40} channels. For a single channel, the steady-state occupancies reflect the mean fraction of time a channel spends in each of the four activatable states. The rates predict that a γ_{40} channel exposed to 10 μM-ACh (see Fig. 2) spends, on the average, 10, 12, 4 and 74% of its time within bursts in vacant, monoliganded, doubly liganded (closed) and open states, respectively. Under similar conditions the rates predict that a γ_{60} channel is usually vacant (Fig. 3), with equivalent occupancy values of 52, 23, 3 and 22%.

Other evidence

There are aspects of the single-channel data other than interval duration distributions that might shed light on the reliability of the rate constant estimates given in Table 2. One prominent prediction from the rates is that even at low [ACh], γ_{60}

channels should produce many fast closures which do not reach half-amplitude (Table 4) and that these unresolved events should give rise to an increase in the variance of the open-channel currents relative to that of the baseline. Figure 12*A* shows histograms of the distribution of the baseline and the open-channel current amplitudes for both γ_{40} and γ_{60} channels. These histograms were fitted by normal distributions (from the mean to 2 pA above the mean). The baseline current had the least variance (0·37 pA^2) followed by γ_{40} open-channel current (mean = 5·4 pA;

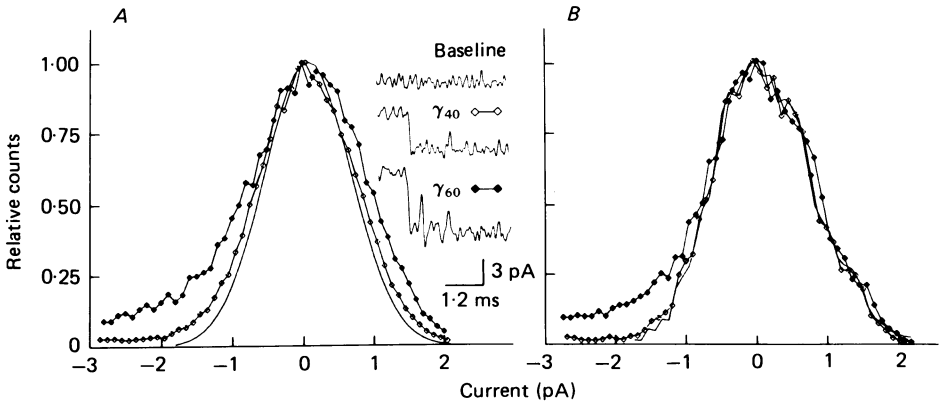

Fig. 12. Amplitude distributions of actual and simulated single-channel currents. Continuous line, baseline current; open symbols, γ_{40} current; filled symbols, γ_{60} current. The current amplitudes have been offset to have a mean of zero. *A*, myocyte currents. Mean γ_{40} amplitude = 5·4 pA; mean γ_{60} amplitude = 7·7 pA; [ACh] = 5 μM. Inset: examples of baseline, γ_{40} and γ_{60} currents. *B*, simulated currents. Data were generated using scheme 1 and the rate constants given in Table 3 (equivalent binding).

variance = 0·50 pA^2) and γ_{60} open-channel current (mean = 7·7 pA; 0·57 pA^2). If most of the excess variance in the open-channel currents arises from 'slow' fluctuations channel conductance (Sigworth, 1985), our data indicate that the larger mean current of γ_{60} channels is accompanied by a larger variance in the 'slow' open-channel noise. More pertinent, the three current distributions have different shapes: the baseline current amplitudes are symmetric about the mean, the γ_{40} current amplitudes are very slightly skewed toward lower values, and the γ_{60} channel current amplitudes are substantially skewed toward lower values. This skew presumably arises from unresolved fast closures (FitzHugh, 1983; Yellen, 1984). In the experiment shown, the concentration of ACh was 5 μM, so most fast closures can be associated with conformational changes in γ_{60} channels rather than channel block by agonist molecules.

The distribution of open-channel current amplitudes are complex functions of the distributions of the open and closed interval durations, the filter characteristics, the sampling frequency, and the peculiarities of 'slow' open-channel current fluctuations. To test whether our rate constant estimates are consistent with the observed skew in the open-channel current amplitude distributions, γ_{40} and γ_{60} channel currents were simulated using the kinetic model of scheme 1 and the rates in Table 3 (equivalent

binding; 5 μM-ACh). The current amplitude histograms produced by the simulation are shown in Fig. 12*B*. The simulated γ_{40} currents are approximately symmetric about the mean, but the simulated γ_{60} current amplitudes are skewed in a manner which is qualitatively similar to those obtained in the data file. We conclude that the characteristics of the excess variance in the γ_{60} (and γ_{40}) open-channel current amplitude distributions are consistent with that predicted from the rate constants.

A second check on the validity of the rate estimates which is independent of interval duration measurement can be obtained from determining the probability that a γ_{40} or γ_{60} channel is open in experiments at very low agonist concentrations. Assuming that desensitization is negligible, the ratio of these experimentally obtained values to the steady-state probability of occupying the open state for one channel (which can be calculated from our rate constant estimates; Fig. 1*C* and the A_2O profiles in Fig.11) should equal the number of activatable channels in the patch. The results were compiled for five patches at 100 nM-ACh. In these patches the probability of being open was $0{\cdot}039 \pm 0{\cdot}020$ (mean $\pm$ S.D.) for γ_{40} channels and $0{\cdot}00055 \pm 0{\cdot}00023$ for γ_{60} channels. From these data we calculate that there were 52 ± 28 (range = 19–91) γ_{40} channels and 13 ± 6 (range = 6–23) γ_{60} channels in each patch. Desensitization would make these values underestimates; the estimated number of γ_{60} may be particularly low because run-down in γ_{60} channel activity after a few minutes exposure to 100 nM-ACh has been reported (Brehm *et al.* 1984).

The estimated number of channels in our patches are reasonable and are similar to those measured for BC_3H1 cells either by rapid perfusion of high [ACh] to outside-out patches (forty-four channels per patch; Brett, Dilger, Adams & Lancaster, 1986) and from single-channel kinetics at low [ACh] (forty-seven channels per patch; Sine & Steinbach, 1986). Thus an erroneous account of the relative number of large- and small-conductance cholinergic channels may be obtained by simply comparing frequencies of channel opening. γ_{60} channels have a lower affinity for ACh than do γ_{40} channels, and given the same number of channels exposed to the same concentration of ACh, γ_{60} channels will open less frequently than will γ_{40} channels.

DISCUSSION

Summary

The predominant kinetic forms of γ_{40} and γ_{60} cholinergic channels in *Xenopus* myocytes differ both in their agonist binding and channel gating properties. The data suggest that (1) ACh molecules bind to γ_{40} channels with almost a 3-fold higher affinity than to γ_{60} channels, and (2) the rates of channel opening and closing are at least 5–10 times faster in γ_{60} channels than in γ_{40} channels. Also, there is some suggestion that there is positive co-operativity in ACh binding to γ_{40}, but not γ_{60}, channels.

Reliability of rate constant estimates

There is no set of activation rate constants which will uniquely account for our main experimental result – the dependence of the apparent channel opening rate, β', on [ACh] (Fig. 9). In order to arrive at our rate constant estimates we made the critical assumption that the kinetics of fast gaps at low [ACh] largely reflect sojourns

in the A_2C state of scheme 1. Previous work indicates that this assumption can be invalid; in chick myotubes (Auerbach & Sachs, 1984) and the mouse BC_3H1 cells (Sine & Steinbach, 1986) there are many classes of short-lived closed states many of which do not represent that A_2C state. In other preparations, including the frog end-plate, the assumption appears to be valid (Colquhoun & Sakmann, 1985).

We have no evidence concerning the identity of fast closures at low [ACh], e.g. measurements of gap amplitudes or of the dependence of gap duration on the nature of the agonist. However, for γ_{40} channels two observations are consistent with the association of most fast gaps with the A_2C state. First, at each [ACh] the patch-to-patch variability in the proportion of fast gaps is small (Tables 1 and 2); the rates of entry into other short-lived closed states which are not associated with gating might be expected to be more variable (Auerbach & Sachs, 1984; Sigworth, 1985). Second, the values of β and the maximum burst P_o estimated from low [ACh] experiments under the assumption that all fast gaps are sojourns in A_2C ($\sim 7000\ s^{-1}$ and 0·96) are very similar to that obtained from high-concentration experiments where no such assumption was made ($\sim 6600\ s^{-1}$ and 0·94). The agreement is less certain for γ_{60} channels because at low [ACh] gaps were too fast and too rarely detected to allow accurate estimates of the fast closed interval distributions.

To summarize, the data clearly indicate that once doubly liganded, γ_{60} channels open faster than γ_{40} channels, and that γ_{60} channels have a lower affinity for ACh than do γ_{40} channels. The quantitative estimates of the activation rate constants given in Table 3 are consistent with our data from 40 nM to 100 μM-ACh but we cannot unequivocally conclude that they are the only set of rates which could account for our data.

Comparison with other single-channel analyses

The kinetics of single ACh-activated channels have been examined in detail in frog end-plate (Colquhoun & Sakmann, 1985), snake end-plate (Leibowitz & Dionne, 1984), mouse BC_3H1 cells (Sine & Steinbach, 1984, 1987), and in *Xenopus* myocytes (Igusa & Kidokoro, 1987). The values of the activation rate constants from these studies have disagreed sharply. For example, the estimated values of β (at 10 °C) are about 100-fold higher in the frog than in the mouse. Our data suggest a basis for the discrepancy in rate constant estimates: frog end-plate channels are γ_{60}-type channels and cholinergic channels in BC_3H1 cells are of the γ_{40} class.

It is difficult to compare quantitatively our activation rate constant estimates with those obtained from the frog and mouse because the experiments were carried out under different conditions, most notably at different temperatures. Moreover, it is difficult to correct for temperature differences using published Q_{10} values for gating rates because these have invariably been derived from macroscopic measurements and are likely to reflect the temperature dependence of a lumped process which includes opening, closing and dissociation. We can, however, pose the following question: how temperature dependent must the gating rates be to make our γ_{60} rates equal those at the frog end-plate and our γ_{40} rates equal those in BC_3H1 cells? Q_{10} values can be calculated for an arbitrary temperature difference, ΔT, by:

$$Q_{\Delta T} = Q_{10}^{\Delta T/10}.$$

With ACh as agonist at the frog end-plate, β and α have been estimated at 31 000 and 700 s^{-1} at 10 °C (Colquhoun & Sakmann, 1985). These would coincide with our γ_{60} rate estimates if β and α had Q_{10}values of 1·2 and 3·4. These Q_{10} values are similar to those estimated for β from the temperature dependence of miniature end-plate current rise times (2·3; Dwyer, 1981) and for α from the spectral characteristics of ACh-induced noise at the frog end-plate (2·6–3·2; Anderson & Stevens, 1973). With ACh as agonist at BC_3H1 cells, β and α have been estimated to be 500 and 35 s^{-1} at 11 °C (Sine & Steinbach, 1987). These would coincide with our γ_{40} rate estimates if β and α had Q_{10} values of 6·8 and 5·9. These high values may be reasonable since Sachs & Lecar (1977) have reported a strikingly steep temperature dependence ($Q_{10} = 5·3$) of the half-power frequency of ACh-induced noise in embryonic chick myotubes. However, the calculated Q_{10} values could be overestimated because frogs and mice operate at different body temperatures; if a ΔT value of 27 °C is used in the above equation, the Q_{10} estimates for γ_{40} β and α become 2·5 and 2·3.

There thus appears to be a reasonably good quantitative agreement between the kinetic properties of *Xenopus* myocyte γ_{60} (H-mode) channels and those at the frog end-plate, and between *Xenopus* myocyte γ_{40} (H-mode) channels and those in BC_3H1 cells. In addition, our data suggest that the gating rates of γ_{60} channels may be less temperature dependent than those of γ_{40} channels.

Igusa & Kidokoro (1987) have also compared the kinetic properties of γ_{40} and γ_{60} cholinergic channels in *Xenopus* myocytes. The burst P_o *vs.* [ACh] data they report are quite similar to ours, but their estimates of the activation rate constants are significantly less than the rates given in Table 3. For example, their proposed values of β for γ_{60} and γ_{40} channels are > 50-fold and > 5-fold slower than ours, respectively. This discrepancy is due to their interpretation of the intermediate closed interval component as representing sojourns in the A_2C state. In our analysis we conclude that this component does not reflect states in the main activation sequence, but that the fastest component does. In their experiments the fastest closed interval component was not resolved, perhaps because the bin width of their interval duration histograms (0·2 ms) was long compared to the time constant of fast gaps.

Implications for channel structure

The differences in conductance and apparent open-channel lifetime between presumed adult and fetal bovine cholinergic channels have been shown to reflect differences in subunit composition (Mishina *et al.* 1986). If a similar swap of subunits provided the only structural difference between *Xenopus* γ_{40} and γ_{60} H-mode channels, our data suggest that in addition to conductance and gating rates, agonist affinity (and perhaps co-operativity in agonist binding) is also affected by the replacement of a γ with an ϵ subunit. Because the rate-limiting barrier to ion permeation is within the electric field of the membrane (Lewis & Stevens, 1979) and the agonist binding sites are on the extracellular surface of the channel, far removed from the membrane surface (Kistler, Stroud, Klymkowsky, Lalancette & Fairclough, 1982), differences in affinity and co-operativity between γ_{40} and γ_{60} channels suggest either that (1) long-range conformational adjustments in the channel protein are occurring as a consequence of subunit replacement, or (2) one or more of the ACh molecules bind to receptor activation sites which can interact with the γ or ϵ subunit.

It is of course possible that differences in subunit composition are only one of a number of structural differences between γ_{60} and γ_{40} channels, and that other differences – e.g. in primary sequence(s), post-translational modifications, or local membrane environment – underlie the differences in agonist binding and/or gating properties between the two types of channel.

Implications for synaptic function

Both early and late in the development of *Xenopus* end-plates there is excellent correlation between end-plate current decay times and the characteristic time constant of ACh-induced noise (Brehm, Steinbach & Kidokoro, 1982). This observation indicates that ACh is rapidly removed from the synaptic cleft by diffusion and hydrolysis, and that the decay of the end-plate current largely reflects the lifetime of doubly liganded forms of the channel. From the rates given in Table 3, end-plates constituted only of γ_{60} channels would give rise to miniature end-plate currents (m.e.p.c.s) which decay ~ 3 times faster than those made up of γ_{40} channels. Furthermore, the faster opening rates for larger-conductance channels suggest that m.e.p.c.s from end-plates containing only γ_{60} channel would have faster rise times than those containing only γ_{40} channels. It is well documented that during development of *Xenopus* neuromuscular synapses, short-lived channels replace long-lived channels and that both the m.e.p.c. decay times (Brehm *et al.* 1982) and rise times (Kullberg, Owens & Vickers, 1985) decrease. It is not clear, however, if the differences in activation kinetics between γ_{60} and γ_{40} channels are sufficient to account for all of the differences in m.e.p.c. shape, and it may be necessary to invoke differences in receptor density, synaptic morphology and/or acetylcholinesterase activity as the bases for differences in m.e.p.c. rise times with development. In addition, it is possible that cholinergic channels at mature synapses have different kinetic properties than the γ_{40} and γ_{60} H-mode channels we have studied in non-synaptic membrane.

The activation rate estimates for γ_{60} and γ_{40} H-mode channels give rise to very different interpretations of the apparent channel open time as viewed in single-channel records at 5 kHz bandwidth. For γ_{40} channels, the rates predict that sojourns in the doubly liganded, closed state are often detected and that the apparent open time (3·4 ms) is only slightly longer than the true open-channel lifetime (2·8 ms). This is not the case for γ_{60} channels, where the rates predict that sojourns in the doubly liganded, closed conformation are quite brief and largely remain undetected. Here the apparent open-channel lifetime ($\sim 800\ \mu$s) overestimates the true open-channel lifetime ($\sim 250\ \mu$s) over 3-fold.

Finally, the quantitative difference in the end-plate current decay for the two conductance forms of channels can be interpreted in terms of the activation rate constants. Although γ_{60} channels close > 10 times faster than γ_{40} channels, after closing they reopen with a higher probability (0·76) than do γ_{40} channels (0·29). Thus the shorter γ_{60} open-channel lifetime is in part compensated by a larger number of openings before dissociation, resulting in about a 3-fold faster decay of the end-plate current.

We thank Jim Neil for writing LPROC, the database manager for single-channel records, and CSIM, the single-channel current simulator. We also thank Fred Sachs for his critical comments and material support (NS-13194). This work was supported by grants to A.A. (MDA, the Whitaker Foundation, NSF BNS-14085) and C.L. (MDA, Career Development Award NS-00836, NS-19139).

REFERENCES

ANDERSON, C. R. & STEVENS, C. F. (1973). Voltage clamp analysis of acetylcholine produced end-plate current fluctuations at frog neuromuscular junction. *Journal of Physiology* **235**, 655–691.

AUERBACH, A. & LINGLE, C. J. (1986*a*). Cholinergic receptors in *Xenopus* myocytes: larger conductance channels have lower affinity for ACh. *Biophysical Journal* **49**, 3a.

AUERBACH, A. & LINGLE, C. J. (1986*b*). Heterogeneous kinetic properties of acetylcholine receptor channels in *Xenopus* myocytes. *Journal of Physiology* **378**, 119–140.

AUERBACH, A. & LINGLE, C. J. (1987). Kinetics of cholinergic channel activation in *Xenopus* myocytes. *Biophysical Journal* (in the Press).

AUERBACH, A. & SACHS, F. (1984). Single channel currents from acetylcholine receptors in embryonic chick muscle: kinetic and conductance properties of gaps within bursts. *Biophysical Journal* **45**, 187–198.

BLATZ, A. & MAGELBY, K. (1986). Correcting single channel data for missed events. *Biophysical Journal* **49**, 967–980.

BREHM, P., KIDOKORO, Y. & MOODY-CORBETT, F. (1984). Acetylcholine receptor channel properties during development of *Xenopus* muscle cells in culture. *Journal of Physiology* **357**, 203–217.

BREHM, P., STEINBACH, J. H. & KIDOKORO, Y. (1982). Channel open time of ACh receptors on *Xenopus* muscle cells in dissociated cell culture. *Developmental Biology* **91**, 93–103.

BRETT, R. S., DILGER, J. P., ADAMS, P. & LANCASTER, B. (1986). A method for the rapid exchange of solutions bathing excised membrane patches. *Biophysical Journal* **50**, 987–992.

COLQUHOUN, D. & HAWKES, A. G. (1977). Relaxation and fluctuations of membrane currents that flow through drug-operated ion channels. *Proceedings of the Royal Society* B **199**, 231–262.

COLQUHOUN, D. & HAWKES, A. G. (1981). On the stochastic properties of single ion channels. *Proceedings of the Royal Society* B **211**, 205–235.

COLQUHOUN, D. & SAKMANN, B. (1981). Fluctuations in the microsecond time range of the current through single acetylcholine receptor ion channels. *Nature* **294**, 464–466.

COLQUHOUN, D. & SAKMANN, B. (1985). Fast events in single-channel currents activated by acetylcholine and its analogues at the frog muscle end-plate. *Journal of Physiology* **369**, 501–557.

COLQUHOUN, D. & SIGWORTH, F. J. (1983). Fitting and statistical analysis of single channel records. In *Single-Channel Recording*, ed. SAKMANN, B. & NEHER, E., New York: Plenum Press.

DIONNE, V. E. (1986). Two kinds of acetylcholine-receptor channels at snake twitch muscle end-plates. *Biophysical Journal* **49**, 4a.

DWYER, T. M. (1981). The rising phase of the miniature endplate current at the frog neuromuscular junction. *Biochimica et biophysica acta* **646**, 51–60.

FITZHUGH, R. (1983). Statistical properties of the asymmetric random telegraph signal, with applications to single-channel analysis. *Mathematical Biosciences* **64**, 75–89.

HAMILL, O. P., MARTY, A., NEHER, E., SAKMANN, B. & SIGWORTH, F. J. (1981). Improved patch-clamp technique for high-resolution current recording from cells and cell-free membrane patches. *Pflügers Archiv* **391**, 85–100.

IGUSA, Y. & KIDOKORO, Y. (1987). Two types of acetylcholine receptor channels in developing *Xenopus* muscle cells in culture: further kinetic analyses. *Journal of Physiology* **389**, 271–300.

JACKSON, M. (1984). Spontaneous openings of the acetylcholine receptor channel. *Proceedings of the National Academy of Sciences of the U.S.A.* **81**, 3901–3904.

KATZ, B. & MILEDI, R. (1972). The statistical nature of the acetylcholine potential and its molecular components. *Journal of Physiology* **224**, 665–699.

KISTLER, J., STROUD, R. M., KLYMKOWSKY, M. W., LALANCETTE, R. A. & FAIRCLOUGH, R. H. (1982). Structure and function of an acetylcholine receptor. *Biophysical Journal* **37**, 371–383.

KULLBERG, R., OWENS, J. & VICKERS, J. (1985). Development of synaptic currents in immobilized muscle of *Xenopus laevis*. *Journal of Physiology* **364**, 57–68.

LEIBOWITZ, M. D. & DIONNE, V. E. (1984). Single-channel acetylcholine receptor kinetics. *Biophysical Journal* **45**, 153–163.

LEONARD, R. J., NAKAJIMA, S., NAKAJIMA, Y. & TAKAHASHI, T. (1984). Differential development of two classes of acetylcholine receptors in *Xenopus* muscle in culture. *Science* **266**, 55–57.

LEWIS, C. A. & STEVENS, C. F. (1979). Mechanism of ion permeation through channels in a

postsynaptic membrane. In *Membrane Transport Processes* 3, ed. STEVENS, C. F. & TSIEN, R. W., pp. 89–103. New York: Raven Press.

MARSHALL, L. M. (1985). Presynaptic control of synaptic channel kinetics in sympathetic neurons. *Nature* **317**, 621–623.

MISHINA, M., TAKAI, T., IMOTO, K., NODA, M., TAKAHASHI, T., NUMA, S., METHFESSEL, C. & SAKMANN, B. (1986). Molecular distinction between fetal and adult forms of muscle acetylcholine receptor. *Nature* **321**, 406–411.

NELSON, D. & SACHS, F. (1979). Single ionic channel observed in tissue-cultured muscle. *Nature* **282**, 861–863.

OGDEN, D. C. & COLQUHOUN, D. (1985). Ion channel block by acetylcholine, carbachol, and suberyldicholine at the frog neuromuscular junction. *Proceedings of the Royal Society* B **225**, 329–355.

ROUX, B. & SAUVE, R. (1985). A general solution to the time interval solution problem applied to single channel analysis. *Biophysical Journal* **48**, 149–158.

SACHS, F. & AUERBACH, A. (1983). Single channel electrophysiology: use of the patch clamp. *Methods in Enzymology* **103**, 147–176.

SACHS, F. & LECAR, H. (1977). Acetylcholine-induced current fluctuations in tissue-cultured muscle cells under voltage clamp. *Biophysical Journal* **17**, 129–143.

SACHS, F., NEIL, J. & BARKAKATI, N. (1982). The automated analysis of data from single ionic channel. *Pflügers Archiv* **395**, 331–340.

SAKMANN, B., PATLAK, J. & NEHER, E. (1980). Single acetylcholine-activated channels show burst-kinetics in the presence of desensitizing concentrations of agonists. *Nature* **286**, 71–73.

SCHEUTZE, S. M. (1980). The acetylcholine channel open time in chick muscle is not decreased following innervation. *Journal of Physiology* **303**, 111–124.

SCHEUTZE, S. M. & ROLE, L. W. (1987). Developmental regulation of the nicotinic acetylcholine receptor. *Annual Review of Neuroscience* **10**, 403–458.

SIGWORTH, F. J. (1985). Open channel noise I. Noise in acetylcholine receptor currents suggests conformational fluctuations. *Biophysical Journal* **47**, 709–720.

SINE, S. M. & STEINBACH, J. H. (1984). Agonists block currents through acetylcholine receptor channels. *Biophysical Journal* **46**, 277–283.

SINE, S. M. & STEINBACH, J. H. (1986). Activation of acetylcholine receptors on clonal mammalian BC3H-1 cells by low concentrations of agonist. *Journal of Physiology* **373**, 129–162.

SINE, S. M. & STEINBACH, J. H. (1987). Activation of acetylcholine receptors on clonal mammalian BC3H-1 cells by high concentrations of agonist. *Journal of Physiology* **385**, 325–359.

SMITH, D. O. (1986). Two populations of acetylcholine receptor channels at the neuromuscular junction of mature and aged rats. *Biophysical Journal* **49**, 4a.

YELLEN, G. (1984). Ionic permeation and blockade in Ca^{2+}-activated K^+ channels of bovine chromaffin cells. *Journal of General Physiology* **84**, 157–186.